Journal Pre-proof

Boosting *in vitro* cartilage tissue engineering through the fabrication of polycaprolactone-gelatin 3D scaffolds with specific depth-dependent fiber alignments and mechanical stimulation

Ângela Semitela, André F. Girão, Carla Fernandes, Gonçalo Ramalho, Susana C. Pinto, António Completo, Paula A.A.P. Marques

PII: S1751-6161(21)00064-3

DOI: https://doi.org/10.1016/j.jmbbm.2021.104373

Reference: JMBBM 104373

To appear in: *Journal of the Mechanical Behavior of Biomedical Materials*

Received Date: 17 November 2020

Revised Date: 13 January 2021

Accepted Date: 28 January 2021

Please cite this article as: Semitela, Â., Girão, André.F., Fernandes, C., Ramalho, Gonç., Pinto, S.C., Completo, Antó., Marques, P.A.A.P., Boosting *in vitro* cartilage tissue engineering through the fabrication of polycaprolactone-gelatin 3D scaffolds with specific depth-dependent fiber alignments and mechanical stimulation, *Journal of the Mechanical Behavior of Biomedical Materials* (2021), doi: https://doi.org/10.1016/j.jmbbm.2021.104373.

Authorship Contribution Statement

Ângela Semitela: Conceptualization; Investigation (fabrication and characterization of the scaffolds; static and dynamic cell cultures); Writing – original draft.

André F. Girão: Conceptualization; Investigation (fabrication of the scaffolds; dynamic cell culture); Writing – review & editing.

Carla Fernandes: Investigation (fabrication of the scaffolds; static and dynamic cell cultures).

Gonçalo Ramalho: Investigation (fabrication of the scaffolds; static and dynamic cell cultures).

Susana C. Pinto: Investigation (μCT analysis)

António Completo: Supervision, Resources, Funding acquisition, Writing - Review & Editing.

Paula A.A.P. Marques: Supervision, Resources, Writing - Review & Editing.

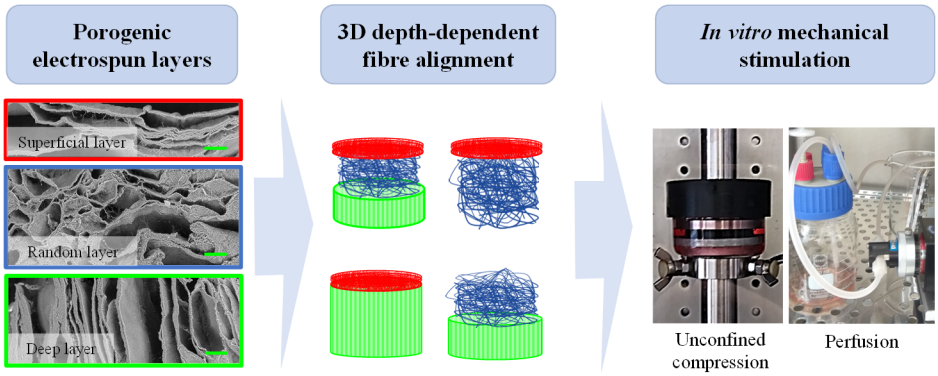

Boosting *in vitro* cartilage tissue engineering through the fabrication of polycaprolactone-gelatin 3D scaffolds with specific depth-dependent fiber alignments and mechanical stimulation

Ângela Semitela[a], André F. Girão[a], Carla Fernandes[a], Gonçalo Ramalho[a], Susana C. Pinto[a], António Completo[a]* and Paula A.A.P. Marques[a]*

[a] Centre of Mechanical Technology and Automation (TEMA), Department of Mechanical Engineering, University of Aveiro, 3810-193 Aveiro, Portugal

*Corresponding author: Paula A.A.P. Marques; E-mail address: paulam@ua.pt

*Corresponding author: António Completo; E-mail address: completo@ua.pt

Abstract

Due to the limited self-healing ability of natural cartilage, several tissue engineering strategies have been explored to develop functional replacements. Still, most of these approaches do not attempt to recreate *in vitro* the anisotropic organization of its extracellular matrix, which is essential for a suitable load-bearing function. In this work, different depth-dependent alignments of polycaprolactone-gelatin electrospun fibers were assembled into three-dimensional scaffold architectures to assess variations on chondrocyte response under static, unconfined compressed and perfused culture conditions. The *in vitro* results confirmed that not only the 3D scaffolds specific depth-dependent fiber alignments potentiated chondrocyte proliferation and migration towards the fibrous systems, but also the mechanical stimulation protocols applied were able to enhance significantly cell metabolic activity and extracellular matrix deposition, respectively.

Keywords: Cartilage tissue engineering; Electrospinning; Depth-dependent properties, Mechanical stimulation

1. Introduction

The intrinsic low density of chondrocytes and the avascularity of the cartilaginous tissue are the two major factors responsible for inhibiting an efficient endogenous regenerative process after trauma (Correa and Lietman, 2017). Furthermore, the standard clinical therapies like autologous chondrocytes injection and microfracture present uncertain success rates, leading recurrently to

unsatisfactory long-term recoveries (Correa and Lietman, 2017; Kock et al., 2012; Makris et al., 2015). In fact, as the newly formed tissue does not retain the zonal disposition of the cartilaginous extracellular matrix (ECM) of the native articular cartilage, the subsequent biochemical and biomechanical properties are manifestly inferior (Correa and Lietman, 2017; Kock et al., 2012). In this regard, tissue engineering (TE) strategies attempt to develop biomimetic constructs capable of recreating the depth-dependent organization of the collagen fibrils, which progress, relatively to the subchondral bone, from perpendicularly aligned in the deepest region, to randomly orientated in the middle zone, to parallel in the superficial region. Indeed, together with the incorporation of cells and mechanical stimulation, recapitulating this specific arrangement in three-dimensional (3D) scaffolds proved to be a decisive factor to generate biomimetic gradients suitable for enhancing chondrocyte response *in vitro* (Johnstone et al., 2013; Luo et al., 2017). 3D scaffolds have been fabricated by freeze-drying (Arora et al., 2015; Fereshteh, 2018), solvent-casting and particulate-leaching (Pedraza et al., 2013) and gas-foaming (Costantini and Barbetta, 2018) methodologies to facilitate the cell distribution and migration as well as, simultaneously, enhance their support while stimulating the production of functional cartilage constructs (Subia et al., 2010; Urbanek et al., 2019; Zhang et al., 2019). Even though these microfabrication techniques were able to recreate hierarchical biochemical and biomechanical arrangements similar to the cartilaginous tissue, they are not proficient to reproduce biomimetic topographic cues (Camarero-Espinosa et al., 2016b). Thus, fibrous scaffolds produced by electrospinning have emerged not only with the purpose of precisely control the scaffolds' nanotopography and architecture, but also to incorporate living cells and growth factors within its structure (Ding et al., 2019; Urbanek et al., 2019; Zhu and Che, 2013). Indeed, with the purpose of creating anisotropic scaffolds that resemble the structural,

topographic and mechanical properties of native cartilage, it is possible to sequentially electrospun different fiber sizes and orientations in a single construct (J.-R. Delcroix et al., 2016; McCullen et al., 2012; Reboredo et al., 2016). While sequential electrospinning has been successfully used for the development of 3D fibrous scaffolds, it may take a long time (from 20 minutes to 20 hours) until the scaffolds reaches a considerable thickness (Sun et al., 2014). Alternatively, post-processing strategies after electrospinning, such as stacking, folding and rolling the two-dimensional electrospun mesh, have attracted substantial interest due to their high flexibility in creating the desired final scaffold shape (Girão et al., 2020, 2018; Munir et al., 2020; Shim et al., 2009; Steele et al., 2014; Tan and Zhou, 2019). The resulting 3D scaffolds had similar morphological features relatively to the native articular cartilage, as well as suitable mechanical properties for TE purposes.

Still, the majority of these anisotropic designs were fabricated using synthetic polymers like polycaprolactone (PCL), which is a biocompatible and biodegradable polymer used in many Food and Drug Administration – approved surgical implants (Bhattarai et al., 2009). Briefly, PCL presents excellent mechanical features, easy processability and physical properties customization, however it shows limited hydrophilicity and natural bio-inductive properties, leading to a sub-optimal cell attachment and proliferation (Powell and Boyce, 2009; Xue et al., 2013; Zhang et al., 2005). Besides its low bio-inductive properties, PCL electrospun scaffolds commonly provide reduced pore sizes, often smaller than the average chondrocyte diameter (between 10 and 20 μm) (Hirsch et al., 1996), which could avert 3D cell migration (Rnjak-Kovacina and Weiss, 2011). To overcome these limitations, approaches such as the incorporation of natural polymers (e.g. gelatin (GEL)) (He et al., 2015; Zheng et al., 2014) to improve bio-inductive properties or the inclusion of polyethylene glycol (PEG) (Baker et al.,

2008; Girão et al., 2020; Wang et al., 2014) microparticles as sacrificial material to optimize the pore size, have been recently combined with considerable improvement in terms of cell attachment, proliferation and infiltration (Semitela et al., 2020). Additionally, wet-electrospinning have also been used to construct 3D fibrous systems with enhanced cell infiltration (Kostakova et al., 2014; Rafiei et al., 2020).

Besides suitable substrates for cell attachment and proliferation, cartilage TE applications also require an appropriate dynamic culture environment – able to induce mechanical stimulation – to generate functional cartilage tissue constructs (Concaro et al., 2008). For instance, unconfined compression has been known to improve ECM production (Remya and Nair, 2020; Zhao et al., 2016), while perfusion systems facilitate nutrient supply/waste removal and induce shear stress mechanical stimulation (Gharravi et al., 2016; McCoy and O'Brien, 2010).

Taking all this into account, in this study, we firstly optimize a microfabrication technique recently reported by our group, where two complementary electrospinning setups were sequentially used to replicate the morphology of each cartilaginous zone (Girão et al., 2018). In this methodology, by adjusting the assembly process of PCL fibrous layers inside a biocompatible graphene oxide-collagen hydrogel it was possible to construct 3D fibrous/porous scaffolds with specific depth-dependent morphological and mechanical features. In the present study, we push forward the potential of this versatile technique as GEL was introduced into the PCL electrospun fibers and PEG sacrificial microparticles were used to augment the pore size of the fibrous network. Then, three specific culture conditions, including static, unconfined compression and perfusion protocols, were applied to four different 3D fibrous/porous geometries for 21 days. The advantages/limitations of each 3D architecture-culture condition

combination were assessed, not only by studying the attachment, proliferation and migration of chondrocytes through the scaffolds, but also by evaluating their ability to produce newly ECM in each particular microenvironment.

2. Materials and Methods

2.1. Materials

PCL with a molecular weight of 80 kDa, GEL from porcine skin, acetic acid, PEG with a molecular weight of 8 kDa, collagen solution from bovine skin (6 mg/mL), articular cartilage progenitor cell line (CP5 (ECACC 08052101)), Dulbecco's modified eagle's medium/nutrient mixture F-12 Ham (1:1) (DMEM/F-12), fetal bovine serum (FBS), penicillin-streptomycin solution (P/S), trypsin/EDTA solution (0.25 %), phosphate-buffered saline (PBS), Mayer's hematoxylin solution, eosin Y solution alcoholic and nuclear fast red-aluminum sulfate solution (0.1%) were purchased from Sigma-Aldrich. Chloroform, resazurin sodium salt, paraformaldehyde (PFA) and alcian Blue 8GX were purchased from ACROS Organics. 2,2,2-trifluoroethanol (TFE) and hexamethyldisilane (HMDS) were purchased from TCI. Ethanol 96 % (v/v) was purchased from PanReac AppliChem and ethanol 100 % (v/v) from ChemLab. Triton X-100 was purchased from Fisher Scientific, Optimum cutting temperature (OCT) compound from Thermo Scientific, and graphene oxide (GO) aqueous dispersion (4.0 mg/mL, water dispersion) from Graphenea.

2.2. Fabrication of the scaffolds

2.2.1. Electrospun layers

PCL and GEL were dissolved separately in TFE at a concentration of 10 % (w/v), stirred vigorously at room temperature (RT) overnight, and mixed at a ratio of 50:50 (PCL:GEL) with 0.2 % (v/v) of acetic acid. A PEG solution (1.5 g/mL) in chloroform was prepared at 50 °C, cooled at RT, and then poured into a 10 mL plastic syringe to be electrosprayed simultaneously with the dry-electrospinning of the PCL+GEL solution (Fig. 1a). It was used a NANON-01A electrospinning setup (MECC), ~~and~~ applying the process parameters defined in Table S1. The resulting meshes of aligned PCL+GEL fibers and PEG microparticles (≈ 130 µm thickness measured with a micrometer) were then washed in a graded series of ethanol aqueous solutions and distilled water to dissolve the PEG microparticles, resulting in porogenic meshes. Two layers were produced using this porogenic electrospun mesh: the superficial layer (fibers parallelly aligned to the scaffold top surface) obtained by cutting circles with 5 mm in diameter with the purpose of pilling them up to achieve the desired height; and the deep layer (fibers perpendicularly aligned to the scaffold top surface) obtained by cutting rectangles with 40 mm in length and a height dependent of the scaffold architecture. These electrospun rectangles were then rolled into spiraled cylinders as illustrated in Fig. 1a. In addition, a set of randomly aligned electrospun layers were produced via wet-electrospinning of a PCL+GEL solution onto a 90 % (v/v) ethanol aqueous solution (Fig. 1a, Table S1). These wet-electrospun meshes were then immersed in graded series of ethanol aqueous solutions and stored in distilled water until further use.

2.2.2. 3D fibrous/porous scaffolds

The electrospun layers were depth-assembled to create four different 3D scaffolds architectures (H1, H2, H3 and H4) following a protocol previously reported by our group (Girão et al., 2018) and represented schematically in Fig. 1b: H1 – containing three layers; H2, H3 and H4 – each containing a different combination of two layers. The ~~different~~ aligned (superficial and deep) and randomly layers were sequentially piled up in a teflon cylindrical mold with 5 mm in diameter and height: deep (2 mm), randomly (2.5 mm) and superficial (0.5 mm) layers for the H1~~,~~; randomly (4.5 mm) and superficial (0.5 mm) layers for H2~~,~~; deep (4.5 mm) and superficial (0.5 mm) layers for the H3 and deep (2.5 mm) and randomly (2.5 mm) layers for the H4. The teflon molds with the assembled layers were then stored at – 20 °C overnight. Afterwards, the frozen 3D structures were removed from the molds and immersed in a GO-collagen hydrogel (Girão et al., 2016) previously placed in a teflon cylindrical mold with 10 mm in diameter and 5 mm high. In this way, it was possible to guarantee the accommodation and support of the layers. The structures were finally freeze-dried (LyoQuest, Telstar) at –80 °C in order to generate the final fibrous/porous scaffolds. A GO-collagen hydrogel-only control was also considered.

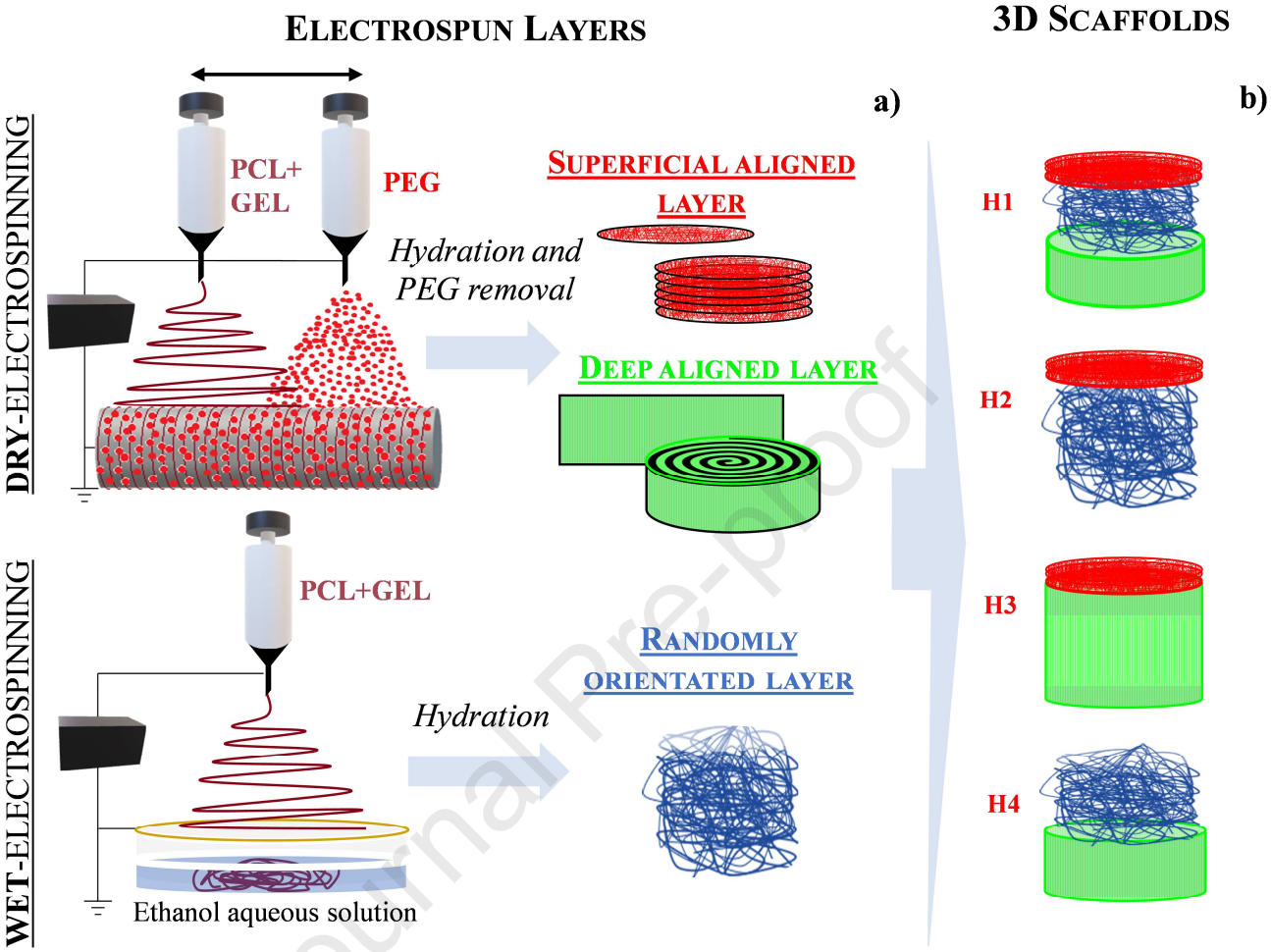

Fig. 1. Schematic representation of the fabrication process of the porogenic electrospun layers (a) and the final 3D fibrous architectures (b). Size: 2 columns and color online only

2.3. Characterization of the scaffolds

2.3.1. Morphology

Scanning electron microscopy (SEM) was used to visualize the morphology of the porogenic electrospun meshes and the cross-sectioned 3D architectures, using a Hitachi SU-70 (15 kV) and a Hitachi TM4000 plus (10 kV). To obtain the cross-sections, the 3D scaffolds were embedded in OCT and sectioned in a cryostat (Leica CM 3050S). Afterwards, the sections were

dehydrated with graded concentrations of ethanol aqueous solutions, treated with HMDS and kept in a fume hood for air drying. Fiber and PEG particle diameter and pore size were determined using Image-Pro Plus software (n > 50). The internal fibrous structure of the scaffolds and the overall layers' orientation was also assessed by micro-computed tomography (µCT), using a Skyscan µCT model 1275 (Brucker), a resolution of 6.5 µm, a voltage of 20 kV and current of 175 µA. The reconstruction, 3D visualization and porosity analysis of the µCT images were performed using respectively the softwares NRecon, CTvox and CTAn (Skyscan, Bruker).

2.3.2. *In vitro* degradation

The *in vitro* degradation analysis of the 3D scaffolds was conducted by incubating the scaffolds, with known weights, in PBS at 37 ºC for 21 days. After 3, 7, 14 and 21 days of incubation, samples (n = 3) of each condition were removed, washed in distilled water and freeze-dried. Afterwards samples were weighted, and the percentage of weight loss was calculated (1).

$$Weight\ loss\ (\%) = \frac{Initial\ weight\ (g) - Final\ weight\ (g)}{Initial\ weight\ (g)} \times 100 \quad (1)$$

2.3.3. Mechanical properties

The compressive properties of the different 3D scaffold architectures were measured under quasi-static unconfined compression in wet conditions at a rate of 0.5 mm/min up to 20 % of strain after a pre-charge of 0.07 N, using a Shimadzu MMT-101 N equipment (Shimadzu Scientific Instruments) with a load cell of 100 N. The compressive moduli of the samples were calculated through the tangent modulus of the linear portion of the stress–strain curves at different strain values (5, 10, 15 and 20 %) (n = 10). The 3D scaffolds were also subjected to

1000 cycles of cyclic sinusoidal unconfined compression in a wet state, at a frequency of 0.5 Hz and up to 10 % strain. The hysteresis ratio was calculated from the ratio of the area between the loading–unloading stress-strain curves and total area under loading stress-strain curve. Moreover, the water absorption capacity of the scaffolds was determined by swelling of freeze-dried scaffolds (with known weights) in distilled water for 24 hours at 37 °C (n = 4).

2.3.4. *In vitro* studies

An articular cartilage progenitor cell line (CP5) was used. Cells were maintained at 37 °C in a humidified atmosphere of 5 % CO_2 in air, in DMEM/F-12, supplemented with 10 % (v/v) FBS and 1 % (v/v) P/S. The medium was refreshed three times a week. Cells were harvested at pre-confluence using trypsin/EDTA solution. The 3D scaffolds were sterilized in 70 % (v/v) ethanol aqueous solution. Then, $7.5x10^5$ cells were seeded onto each scaffold followed by incubation at 37 °C for 2 hours. A negative control, a scaffold without cells, was considered for each architecture. After an initial attachment period of 5 days, cell-laden scaffolds were subjected to unconfined compression on a developed bioreactor (Bandeiras et al., 2015) (Fig. S1a) or to perfusion (Fig. S1b and c). For the unconfined compression protocol, a total of 12 cell-seeded scaffolds (3 scaffolds of each architecture) were placed in the bioreactor and subjected to dynamic unconfined compression regime: 2 hours of sinusoidal compression (0.5 Hz, 0 – 10 % strain) and 10 hours of rest. The stimulation regime was repeated twice a day for 16 days. For the flow perfusion protocol, a total of 12 scaffolds (3 scaffolds of each architecture) were placed in the culture chamber and continuously perfused at a flow rate of 0.75 mL/min per scaffold for 16 days (Fig. S1c). Three static controls of each architecture were placed and cultured in the incubator for the remaining 16 days. For both protocols, the culture medium was refreshed two

times a week. Cell viability was calculated based on the metabolic activity of the cell-laden scaffolds after 1, 4, 7, 14 and 21 days of culture measured by a resazurin method. Briefly, a resazurin solution (0.1 mg/mL in PBS) was added to fresh medium at a final concentration of 10 % (v/v). Scaffolds were incubated in this solution at 37 ºC for 5 hours in the dark, after which 100 µL per well was transferred to a 96-well plate and absorbance (Abs) at 570 and 600 nm was measured in a microplate reader (Synergy HTX). For each day, final absorbance values for individual samples were calculated as the ratio Abs570/Abs600 nm minus the Abs570/Abs600 nm ratio of a negative control (scaffold without cells). The absorbance values of cells incubated in the tissue culture polystyrene on the first time point were taken as 100 % and cell viability calculated as a percentage of these control values. Cell adhesion after 1 day of culture was assessed via SEM visualization following the protocol previously described. After ~~the~~ 21 days of culture, the dynamically stimulated scaffolds, as well as the respective static controls were fixed in 4 % (w/v) PFA in PBS, embedded in the OCT and sectioned transversally in a cryostat (Leica CM 3050S). Afterwards, several scaffolds' sections were stained with hematoxylin and eosin solutions to highlight in purple-blue the cells in the scaffolds anisotropic layers and Alcian Blue (1 % (w/v) in 3 % (v/v) acetic acid – pH 2.5) and nuclear fast red for glycosaminoglycan (GAG) detection, mounted and visualized in an optic microscope (Nikon Eclipse LV150).

2.3.5. Statistical analysis

All the quantitative data are expressed as mean ± standard deviation. Statistical significance was determined, using OriginLab, by performing One-way analysis of variance (ANOVA), followed

by post hoc Tukey's test, except for viability assays, where a One-way (ANOVA) with repeated measures was also used. Significance was accepted at *p*-value inferior to 0.001, 0.01 and 0.05.

3. Results and Discussion

3.1. Morphology of the 3D anisotropic scaffolds

Uniform and smooth fibers of PCL+GEL were obtained independently of the electrospinning modality used, leading to the fabrication of defect free fibrous networks with similar average fiber diameters (0.55 ± 0.16 µm and 0.52 ± 0.11 µm for dry and wet-electrospun meshes, respectively) (Fig. S2c and e). The presence of GEL in the polymeric mixture is known to diminish the electrospun fibers' size and enhance their hydrophilicity (Girão et al., 2018; Semitela et al., 2020), resulting in a beneficial impact on cell behavior (Ke et al., 2017; Sheng et al., 2019; Strobel et al., 2018; Zhang et al., 2005). One of the limitations of the electrospun meshes is their reduced inter-fiber spacing, leading to a deficient cell penetration and low nutrient diffusion and waste removal. Accordingly, earlier reports have shown an average pore size of 4 to 5 µm for this polymeric blend composition, and a consequent limited cell infiltration (Feng et al., 2019; Semitela et al., 2020). In this work, two pore enlargement strategies were employed: the introduction and subsequent removal of a sacrificial agent (PEG) for the superficial and deep-aligned layers, and the fabrication of a randomly oriented fibrous layer via wet-electrospinning. Regarding the first approach, the simultaneous electrospinning/electrosprayed procedure resulted in PEG microparticles with a spherical shape and a broad size distribution (27.21 ± 16.53 µm) homogeneously distributed throughout the

PCL+GEL electrospun mesh (Fig. S2a and b). After their removal, large inter-fiber spaces were created across the electrospun fibrous structure (17.64 ± 6.99 µm), generating, consequently, a higher pore percentage within the 15 to 20 µm range (35 %; Fig. S2d), as previously reported (Semitela et al., 2020). Likewise, the second pore enlargement approach – where PCL+GEL electrospinning was performed onto a liquid collector – generated an average pore size of 15.72 ± 6.12 µm, with the higher percentage of pores within the 10 to 15 µm range (37 %; Fig. S2e and f). Both pore enlargement strategies generated similar pore size values, resulting in porogenic meshes with a nearly 4-fold increase in pore size from the referred pristine PCL+GEL meshes, previously reported (Semitela et al., 2020). It should be emphasized that, given the average chondrocyte diameter is around 10-20 µm (Hirsch et al., 1996), more than 80% of pores present on both aligned and random porogenic PCL+GEL layers should be compatible with the cell migration.

The SEM images of cross-sections of the 3D scaffolds (Fig. 2), as well as the µCT 3D reconstitution (Fig. 3), confirmed the successful assembly of the different combination of fibrous arrangements, displaying depth-dependent fiber orientation. It is expected that these fibrous zonal architectures provide topographic cues for cell attachment, spreading and migration, resulting in specific cellular organization and zonal ECM production (Camarero-Espinosa et al., 2016a). Accordingly, the SEM images (Fig.2) show nanofibrous membranes stacked and aligned parallelly to the surface in the superficial layer, while the random layer is composed by arbitrarily positioned and tangled fibers, and most of the fibers present on the deep layer are positioned perpendicularly to the surface. The described fiber orientation influences the porosity, therefore the superficial layer displays low porosity values of 29.1 ± 7.1 %, lower than the middle and deep layers with present porosity values of 53.1 ± 6.9 % and 55.2

± 3.1 %, respectively, as determined from the µCT 3D images (Fig.3). Indeed, and as expected, the 3D foam-like morphology of the middle layer and the hollow spaces between the 3D concentric walls of the deep layer were able to boost the porosity of these components. It is important to notice that the porosity values presented could be underestimated since there may be additional nanoporosity, which is characteristic of electrospun meshes, that was not accounted due to the equipment's limit of the resolution. Besides the fibrous structure, it is also visible the GO-collagen porous system involving the fibrous layers (Fig. 2, Fig. 3 and Fig. S3a and b). This network was necessary to assure the successful assembly and supporting of the different oriented layers. Furthermore, the biocompatibility as well as the high porosity (74.1 ± 4.3 %), pore interconnectivity and size – ranging from 20 to 100 µm (Fig. S3c) – rendered to the GO-collagen system not only an increased availability of cell migration paths, but also an enhanced water uptake proficient to facilitate nutrient supply, waste removal and deformation recovery upon compression (Girão et al., 2016).

3.2. *In vitro* degradation of the 3D scaffolds

Given that dynamics of tissue regeneration, a scaffolding material should degrade over time, giving way to new cartilage tissue in vivo in order to allow full restoration of native tissue structure and function (Zhang et al., 2019). So, *in vitro* degradation studies were performed to assess the biodegradability of the 3D scaffolds, and the results are displayed in Fig. S4. A weight loss of nearly 10 % was detected after 3 days of incubation for all scaffold architectures and the GO-collagen network. After 21 days of incubation, this value was significantly higher (≈ 25 %), suggesting an overall gradual biodegradation of the 3D scaffolds. Given that no significant differences were found between the four scaffold architectures and GO-collagen

hydrogel, the weight loss was mainly attributed to the porous portion of the 3D scaffolds. Still, previous reports have shown that in a similar PCL+GEL system a significant amount of GEL was leaked into the medium, so possible GEL dissolution from the electrospun layers can not be excluded (Semitela et al., 2020).

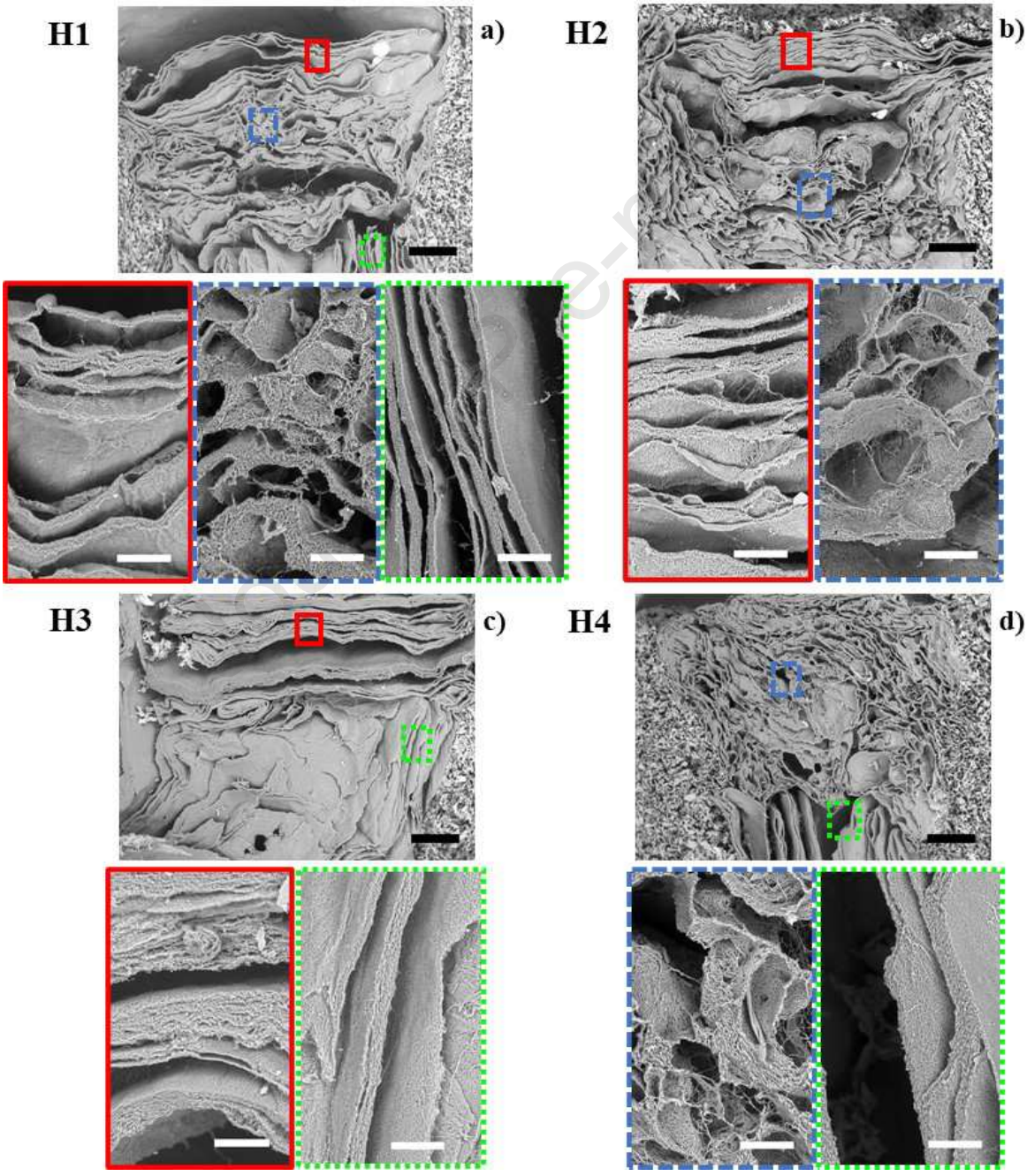

Fig. 2. SEM images of the 3D scaffold cross-sections: H1 architecture with 3 layers (superficial (red – solid line), random (blue – dashed line), deep (green – dotted line)), H2 architecture with 2 layers (superficial, random), H3 architecture with 2 layers (superficial, deep) and H4 architecture with 2 layers (random, deep). Scale bars: black: 500 µm; white: 100 µm. Size: 1.5 columns and color online only

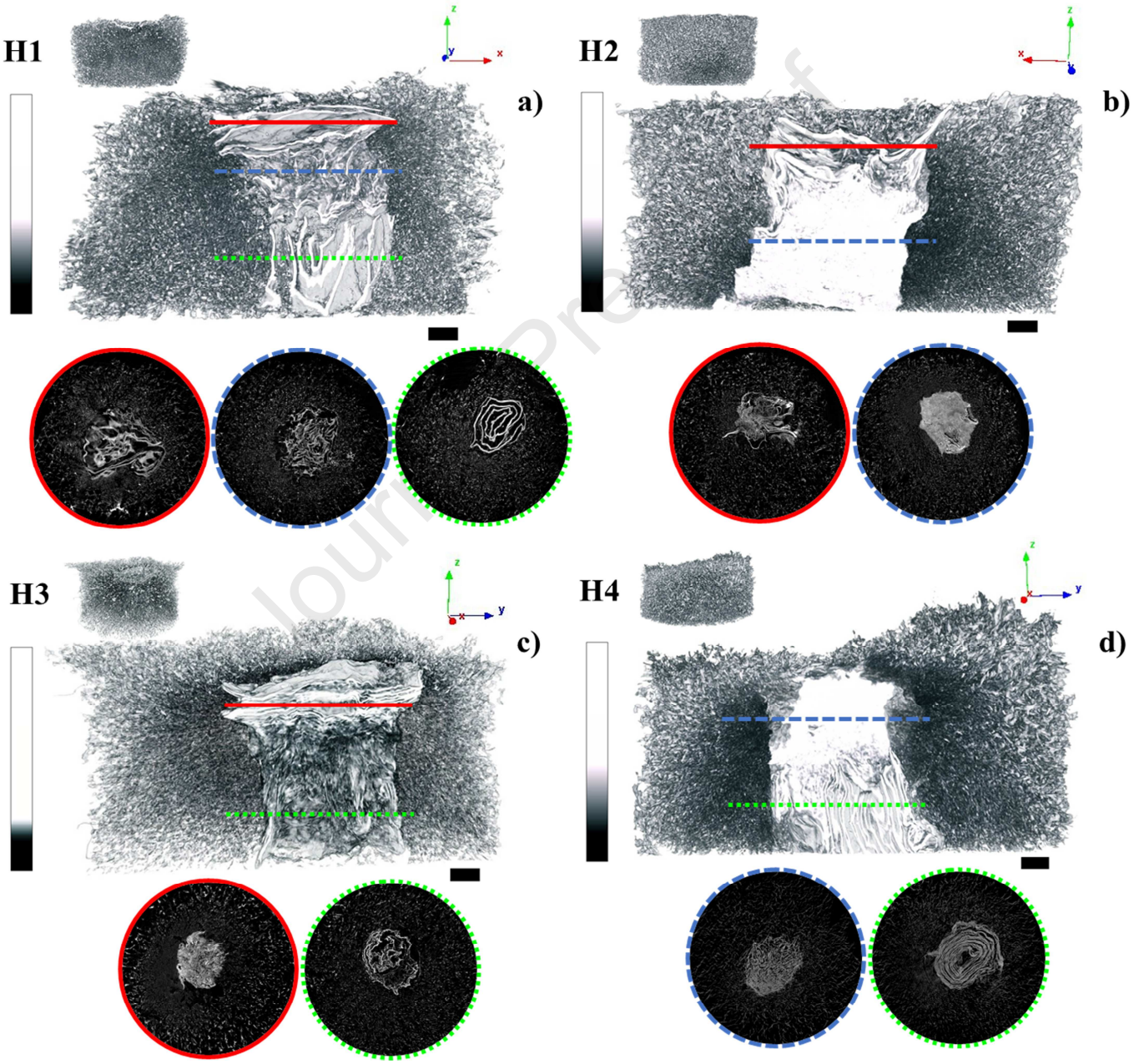

Fig. 3. μ-CT 3D reconstitution of the scaffolds H1 (a), H2 (b), H3 (c) and H4 (d), the respective transversal cross-sections and the segmented 2D slices of each layer (superficial (red – solid line), random (blue – dashed line), deep (green – dotted line)). Metric scale bar: 1 mm. Color scale bar: lighter intensity in grey color represents areas with higher density. Size: 2 columns and color online only

3.3. Mechanical assessment of the 3D scaffolds

The 3D scaffolds' mechanical and swelling properties play a major role on the TE cartilage function, since the native tissue resistance to compression derives from the proteoglycan matrix swelling constriction imposed by the collagen fiber network (Franke et al., 2007). So, the mechanical response of the scaffolds to quasi-static unconfined compressive loading up to 20 % strain, displayed in Fig. 4 and Table S2, was assessed in a swollen state, as these conditions reflect more closely the native physiological environment. All scaffolds architectures displayed linear regimes for the strain interval applied (Fig. 4a). Differences in the mechanical behavior of the 3D scaffolds were observed, mainly at 20 % strain (Fig. 4b and Table S2). H4 architecture, in particular, possessed a significantly higher compression modulus at 20 % strain (41.13 ± 14.11 kPa) than the remaining architectures (29.94 ± 3.16 kPa for H1, 27.91 ± 4.19 kPa for H2 and 27.30 ± 3.58 kPa for H3) which can be attributed to higher water absorption ratio of this architecture (Fig. 4c and Table S3). In fact, H4 displayed the highest water absorption ratio (28.76 ± 2.06 %) after 24 hours in distilled water. The higher fiber-fiber distance in the random layer and the higher amount of spaces between the concentric fibrous branches of the electrospun spiral of the deep layer found on this architecture might be responsible for the increased water uptake, and correspondent higher compression modulus (Girão et al., 2018). In the other hand, the lower compression moduli of the remaining architectures can be attributed to the lower water uptake of the superficial layer, due to its characteristic high fiber packing density (22.82 ± 1.85 % for H1, 23.88 ± 1.00 % for H2 and 24.36 ± 1.11 % for H3 after 24 hours in distilled water; Fig. 4c and Table S3). These compression moduli values, however, are

substantially inferior to the reported for similar PCL only-based anisotropies (40.69 to 85.42 kPa (Girão et al., 2018) and 152.5 ± 42.2 kPa (McCullen et al., 2012)), despite their improved swelling capacity. It is possible that the resistance to compression of these structures may have been compromised by the increased pore size of the layers as well as the incorporation of GEL, which is consistent with previous reports (Jung et al., 2015; Steele et al., 2014; Zhang et al., 2014). Still, it should be noted that while these features might be somewhat detrimental to the 3D scaffolds mechanical response, ~~they will~~ it is expected that they could trigger ~~an expected~~ improved cell response, in terms of chondrocyte attachment and migration.

Considering the complex anatomy and physiology of native cartilage coupled with the wide range of reported experimental conditions, the Young's modulus of the cartilaginous tissue ranges from 0.1 to 5 MPa (Arora et al., 2015; McCullen et al., 2012; Steele et al., 2014), which are significantly higher than the compression moduli reported here. Nonetheless, it has been stated that in *in vivo* conditions scaffolds with lower compression moduli favor chondrogenesis, while stiffer substrates are prone to stimulate chondrocyte dedifferentiation (Schuh et al., 2010). Accordingly, in the current study, the developed scaffolds displayed favorable mechanical properties for maintenance of the chondrogenic phenotype, suggesting its potential for cartilage TE.

Given that native articular cartilage is subjected to conditions of repeated loading, cyclic unconfined compression was applied to the 3D scaffolds, to assess their ability to withstand cyclic loading and their energy dissipation potential (Arora et al., 2015). The stress-strain curves after 1, 10, 100 and 1000 cycles for the 3D scaffolds up to 10 % strain are displayed in Fig. S5. All scaffold architectures possessed viscoelastic behavior with significant energy loss

through cycles 1 to 1000. The energy dissipation of the 3D scaffolds, calculated through hysteresis ratio, ranged between 25 and 62 %, which is consistent with the range reported to native articular cartilage (Malekipour et al., 2013). This parameter plays a crucial role on preventing cartilage damage (Arora et al., 2015). H4 architecture displayed the highest peak stresses, which is consistent with the quasi-static unconfined compression results.

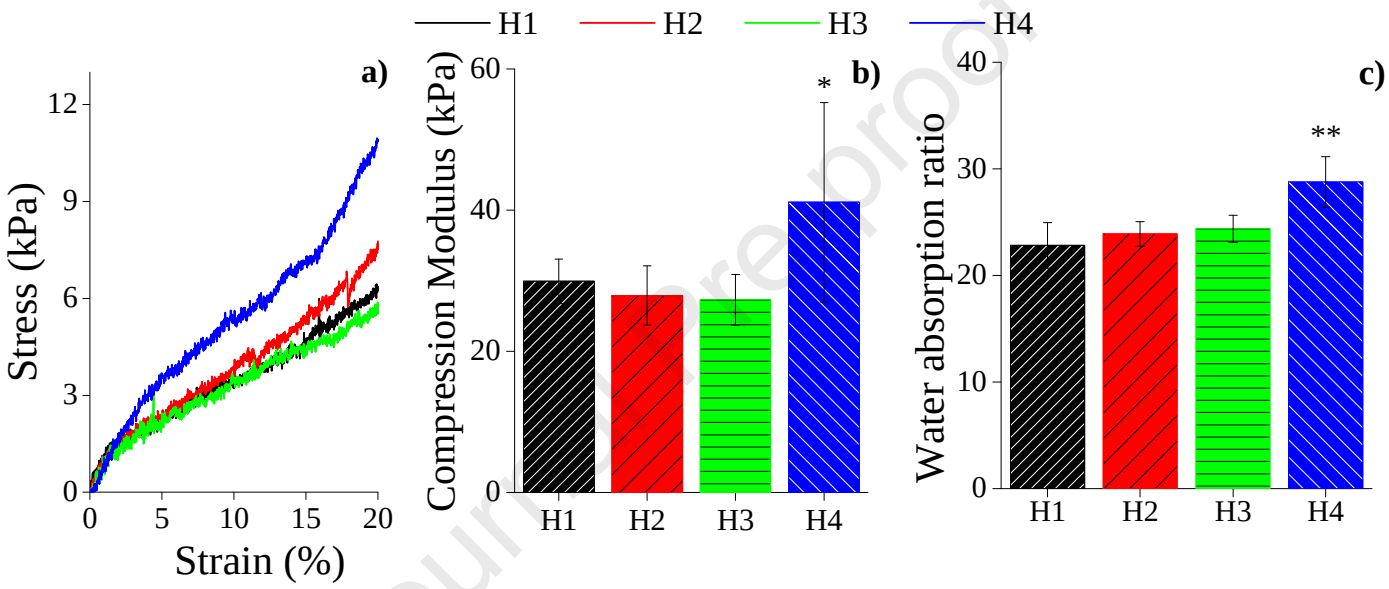

Fig. 4. Compression properties of the 3D scaffolds. (a) stress-strain curves; (b) compression moduli at 20 % strain (n = 10) and, (c) water absorption ratio after 24 hours in distilled water (n = 4). Statistical analysis by One-way ANOVA followed by post hoc Tukey's test; *p <0.05, **p <0.01. Size: 2 columns and color online only

3.4. *In vitro studies*: cytocompatibility and mechanical stimulation of the 3D scaffolds

Articular cartilage progenitor cell response to the 3D scaffolds was firstly evaluated in static conditions. Cells adhere and spread well through the top surface of all scaffold architectures, exhibiting multiple filopodia attached to the nanofibers (Fig. S5 and Fig. S6). Similarly to previous studies, (Girão et al., 2020; Semitela et al., 2020), this typical phenotype occurs during

early stages of the culture, when the cells still present an undifferentiated state. A gradual increase of the percentage of viable cells was observed throughout the culture period under static conditions (Fig. 5), demonstrating the potential of these anisotropic structures to support the articular cartilage progenitor cells attachment, viability and continuous proliferation up to 3 weeks. In reality, such a beneficial impact was expected particularly due to GEL presence (Davidenko et al., 2016; Zhang et al., 2005), and it has been in fact confirmed for this cell line (Semitela et al., 2020). Additionally, pore enlargement of the fibrous structure allowed considerable 3D cell migration, and correspondent higher proliferation rate (Semitela et al., 2020; Wang et al., 2014), which was confirmed by the visible nearly homogeneous cell distribution throughout each layer of the scaffolds, depicted in Fig. 6 and Fig. S7. Interestingly, more cells were found on the randomly aligned layer, regardless of the architecture, suggesting that the randomly-oriented fibers constituted an enhanced support for cell attachment and migration (Fig. 6 and Fig. S7). Following this trend, the absence of a random layer on the H3 architecture resulted in the lowest percentage of metabolic active cells (Fig. 5). This was also consistent with hematoxylin-eosin staining of the cell-seeded H3 architecture (Fig. S7), where fewer cells were found. On the contrary, the H1 and H4 geometries exhibited the highest percentage of metabolic active cells at the end of the 3 weeks with values around 30% (Fig. 5).

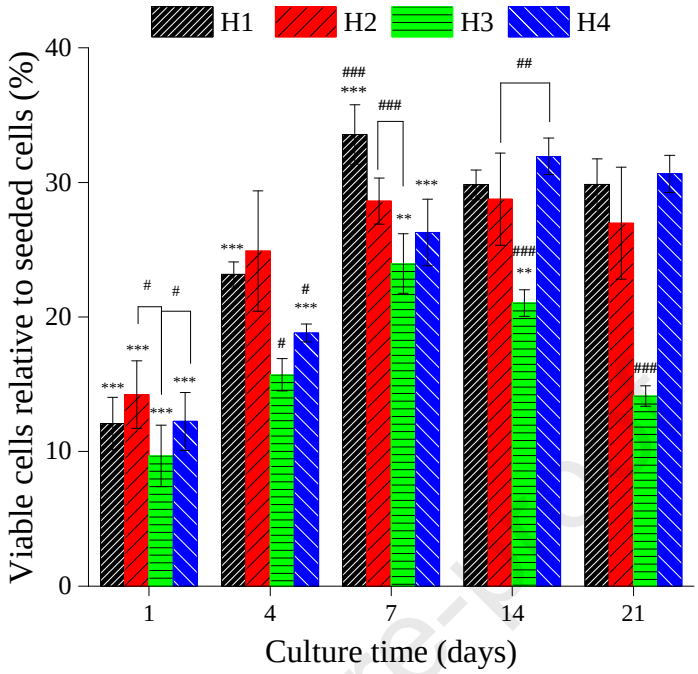

Fig. 5. Percentage of viable articular cartilage progenitor cells seeded on the 3D scaffolds after 1, 4, 7, 14 and 21 days of culture under static conditions (n = 3). Statistical analysis by One-way ANOVA with repeated measures followed by post hoc Tukey's test: ***$p < 0.001$, **$p < 0.01$, where * represents statistical significant differences for each architecture over culture time; and by One-way ANOVA followed by post hoc Tukey's test: $^{###}p < 0.001$, $^{##}p < 0.01$, $^{#}p < 0.05$, where # denotes statistical significant differences between architectures in each time point. Size: single column and color online only

Regarding the mechanical stimulation, whose results are displayed in Fig. 6, Fig. 7 and Fig. S7, it was possible to infer that both mechanical stimulation protocols significantly improved cell response in most of the scaffold architectures (Fig. 7). Indeed, a clear statistically significant difference between cell-laden H1, H2 and H3 architectures under static and unconfined compressed environments was observed, which was corroborated by the cell distribution data (Fig. 6 and Fig. S7). On the contrary, there was no statistically significant differences on the percentage of viable cells of cell-seeded H4 architecture between both conditions (Fig. 7). Despite the significant increase in cell viability under unconfined compression, H3 architecture still promoted the lowest proliferation rate. Even so, while cyclic unconfined compression

stimulation protocol was beneficial for cell proliferation, it was under perfusion that the higher proliferative rate was observed for all geometries (Fig. 7). Indeed, statistically significant differences were observed between the perfused and both static and unconfined compressed environments. In fact, perfusion bioreactor systems have been known to create a more homogeneous microenvironment than static or unconfined compression, facilitating nutrient supply and, therefore, tissue growth (Concaro et al., 2008; Gharravi et al., 2016; Levorson et al., 2014; McCoy and O'Brien, 2010; Silva et al., 2010; Tarng et al., 2012). Under these conditions, a nearly 2-fold increase was observed on the percentage of metabolic active cells of the cell-laden H3. Furthermore, no statistically significant differences were observed in cell viability between H2, H3 and H4 architectures. H1 architecture, on the other hand, displayed the lowest cell viability under perfused conditions. This is also consistent with the findings obtained though the hematoxylin-eosin staining (Fig. 6 and Fig. S7). On the other hand, while a perfused environment improved cell proliferation and migration, unconfined compression accelerated ECM production – GAG. Indeed, GAG staining, displayed in Fig. S8, was more pronounced on the samples subjected to unconfined compression, suggesting an apparent higher GAG deposition, which is in agreement with several reports (Jeon et al., 2012; Sawatjui et al., 2018; Wang et al., 2009). As a matter of fact, given that chondrocytes normally reside in a dynamic mechanical environment, the presence or the absence of mechanical stimuli, in this case unconfined compression, can have a large influence in chondrocyte biosynthesis *in vivo* and matrix remodeling (Jeon et al., 2012). Since the cell line used in this study was initially undifferentiated, it can be inferred that this stimulation protocol stimulated first their differentiation towards a chondrogenic phenotype, and then the biosynthetic activity. This is also corroborated by the reaction force results of the 3D cell-seeded scaffolds under cyclic

unconfined compression, shown in Fig. S8, where an increase of the reaction force is observed after 200 hours of stimulation, attributed to an increase of the biomechanical strength of the 3D scaffolds (Bandeiras and Completo, 2017; Sawatjui et al., 2018; Wang et al., 2019). Taking this in account, an effective approach to improve both cell proliferation and ECM deposition would be to apply simultaneously perfusion and unconfined compression to the cell-laden 3D scaffolds.

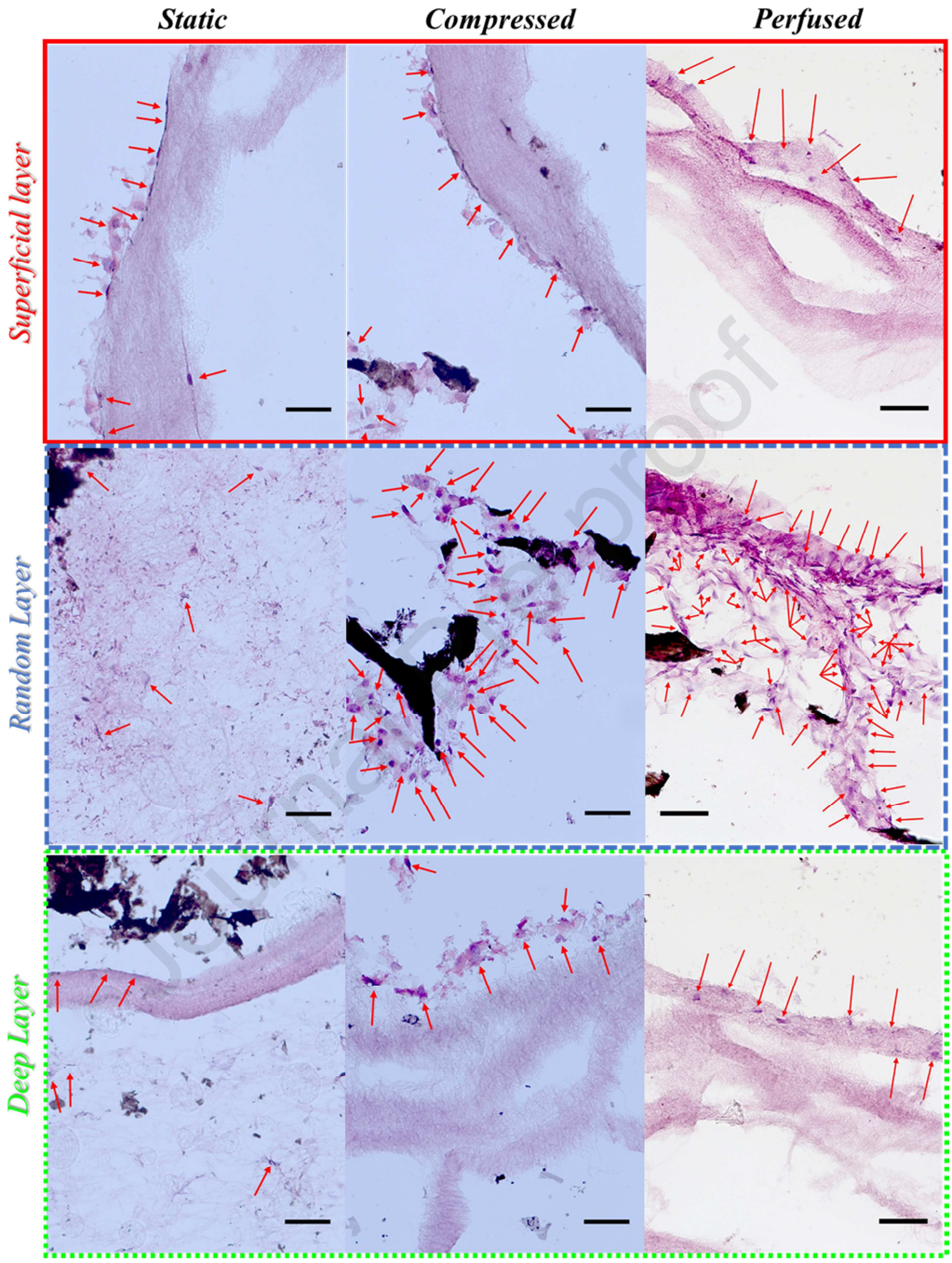

Fig. 6. Images of hematoxylin-eosin stained articular cartilage progenitor cells seeded on the superficial (red – solid line), random (blue – dashed line) and deep (green – dotted line) layers of the H1 scaffold after 21 days of culture under static, unconfined compressed and perfused conditions. The arrows highlight the cells. Scale bars: 50 μm. Size: 1.5 columns

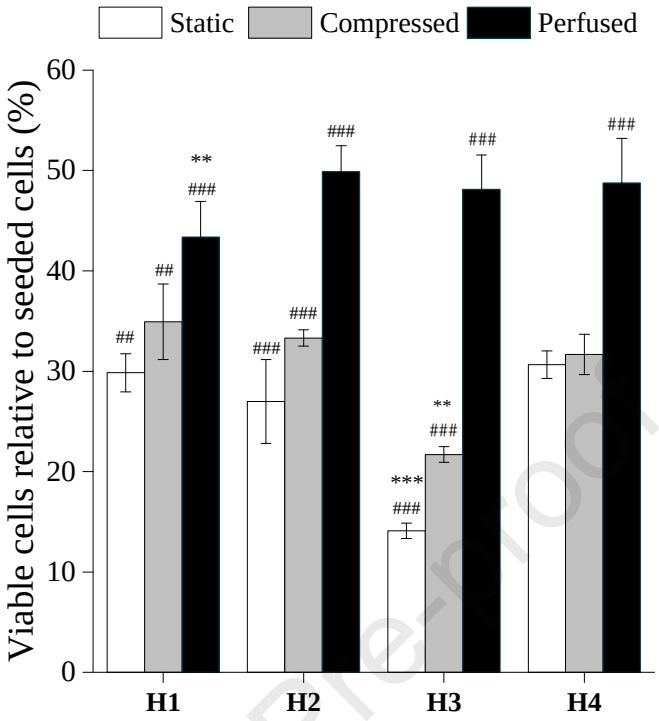

Fig. 7. Percentage of viable articular cartilage progenitor cells seeded on the 3D scaffolds under static, unconfined compressed and perfused environment (5 days static plus 16 days of mechanical stimulation) after 21 days of culture (n = 3). Statistical analysis by One-way ANOVA followed by post hoc Tukey's test: $^{###}p < 0.001$, $^{##}p < 0.01$, $^{#}p < 0.05$, $***p < 0.001$, $**p < 0.01$, where # denotes statistical significant differences between tested environments in each architecture and * denotes statistical significant differences between architectures in each culture environment. Size: single column and color online only

Ultimately, the results presented in this work demonstrated the potential of the developed 3D scaffolds, especially the H1 and H4 architectures, to offer suitable mechanical support, and to promote cell proliferation and migration not only under dynamic conditions, particularly under perfusion, but also in static conditions, rendering them well-suited for cartilage TE applications. Despite the promising results reported here, further *in vitro* and *in vivo* investigations are required to validate their biological efficacy for cartilage TE applications. Furthermore,

optimization of the stimulation protocols should be procured for both bioreactor systems to achieve the optimal environment conditions for enhanced cell response.

4. Conclusions

3D fibrous scaffolds were designed with different depth-dependent alignments of PCL+GEL porogenic fibrous meshes in order to mimic the functional fiber arrangement of the native articular cartilage and to create specific-zonal biochemical and biomechanical properties. Our analysis demonstrated that these scaffolds not only overcame common limitations associated with PCL electrospun scaffolds by facilitating cell attachment and migration, but also the specific fiber alignments generated different mechanical behaviors and, consequent, cell responses with and without mechanical stimulation environments. In particular, the combination of randomly and vertically aligned fibers showed the highest potential for cartilage TE applications. Furthermore, perfusion accelerated substantially cell proliferation and unconfined compression stimulated GAG deposition, suggesting that the simultaneous application of both stimulation protocols could be an alternative for functional cartilage tissue formation.

Acknowledgements

This work was supported by the Portuguese funding of Program COMPETE-FEDER, Programa Operacional Competitividade e Internacionalização through the projects POCI-01-0145-FEDER-028424 and CENTRO-01-0145-FEDER-022083. Also by Fundação para a Ciência e Tecnologia I.P. (FCT, IP) through the projects PTDC/EME-SIS/28424/2017, UIDB/00481/2020 and UIDP/00481/2020. The authors thank to FCT for the PhD grants SFRH/BD/133129/2017

and SFRH/BD/130287/2017. The authors would also like to thank the valuable input of Dr. Nuno Almeida and Dr. Nathalie Barroca.

REFERENCES

Arora, A., Kothari, A., Katti, D.S., 2015. Pore orientation mediated control of mechanical behavior of scaffolds and its application in cartilage-mimetic scaffold design. J. Mech. Behav. Biomed. Mater. 51, 169–183. https://doi.org/10.1016/j.jmbbm.2015.06.033

Baker, B.M., Gee, A.O., Metter, R.B., Nathan, A.S., Marklein, R.A., Burdick, J.A., Mauck, R.L., 2008. The potential to improve cell infiltration in composite fiber-aligned electrospun scaffolds by the selective removal of sacrificial fibers. Biomaterials 29, 2348–2358. https://doi.org/10.1016/j.biomaterials.2008.01.032

Bandeiras, C., Completo, A., 2017. A mathematical model of tissue-engineered cartilage development under cyclic compressive loading. Biomech. Model. Mechanobiol. 16, 651–666. https://doi.org/10.1007/s10237-016-0843-9

Bandeiras, C., Completo, A., Ramos, A., Rufino, A.T., Ribeiro, M., Ferreira, J.P., Mendes, A.F., 2015. Tissue Engineered Cartilage in Unconfined Compression: Biomechanical Analysis. Mater. Today Proc. 2, 355–364. https://doi.org/10.1016/j.matpr.2015.04.032

Bhattarai, N., Li, Z., Gunn, J., Leung, M., Cooper, A., Edmondson, D., Veiseh, O., Chen, M.H., Zhang, Y., Ellenbogen, R.G., Zhang, M., 2009. Natural-synthetic polyblend nanofibers for biomedical applications. Adv. Mater. 21, 2792–2797. https://doi.org/10.1002/adma.200802513

Camarero-Espinosa, S., Rothen-Rutishauser, B., Foster, E.J., Weder, C., 2016a. Articular cartilage: From formation to tissue engineering. Biomater. Sci. 4, 734–767.

https://doi.org/10.1039/c6bm00068a

Camarero-Espinosa, S., Rothen-Rutishauser, B., Weder, C., Foster, E.J., 2016b. Directed cell growth in multi-zonal scaffolds for cartilage tissue engineering. Biomaterials 74, 42–52. https://doi.org/10.1016/j.biomaterials.2015.09.033

Concaro, S., Gustavson, F., Gatenholm, P., 2008. Bioreactors for Tissue Engineering of Cartilage, in: Kasper, C., van Griensven, M., Pörtner, R. (Eds.), Bioreactor Systems for Tissue Engineering. Springer, Berlin, pp. 125–144. https://doi.org/10.1007/10_2008_10

Correa, D., Lietman, S.A., 2017. Articular cartilage repair: Current needs, methods and research directions. Semin. Cell Dev. Biol. 62, 67–77. https://doi.org/10.1016/j.semcdb.2016.07.013

Costantini, M., Barbetta, A., 2018. Gas foaming technologies for 3D scaffold engineering, in: Deng, Y., Kuiper, J. (Eds.), Functional 3D Tissue Engineering Scaffolds. Elsevier, Newark, DE, United States, pp. 127–149. https://doi.org/10.1016/B978-0-08-100979-6.00006-9

Davidenko, N., Schuster, C.F., Bax, D. V., Farndale, R.W., Hamaia, S., Best, S.M., Cameron, R.E., 2016. Evaluation of cell binding to collagen and gelatin: a study of the effect of 2D and 3D architecture and surface chemistry. J. Mater. Sci. Mater. Med. 27, 148. https://doi.org/10.1007/s10856-016-5763-9

Ding, J., Zhang, J., Li, J., Li, D., Xiao, C., Xiao, H., Yang, H., Zhuang, X., Chen, X., 2019. Electrospun polymer biomaterials. Prog. Polym. Sci. 90, 1–34. https://doi.org/10.1016/j.progpolymsci.2019.01.002

Feng, B., Wang, S., Hu, D., Fu, W., Wu, J., Hong, H., Domian, I.J., Li, F., Liu, J., 2019. Bioresorbable electrospun gelatin/polycaprolactone nanofibrous membrane as a barrier to prevent cardiac postoperative adhesion. Acta Biomater. 83, 211–220.

https://doi.org/10.1016/j.actbio.2018.10.022

Fereshteh, Z., 2018. Freeze-drying technologies for 3D scaffold engineering, in: Deng, Y., Kuiper, J. (Eds.), Functional 3D Tissue Engineering Scaffolds. Elsevier, Newark, DE, United States, pp. 151–174. https://doi.org/10.1016/B978-0-08-100979-6.00007-0

Franke, O., Durst, K., Maier, V., Göken, M., Birkholz, T., Schneider, H., Hennig, F., Gelse, K., 2007. Mechanical properties of hyaline and repair cartilage studied by nanoindentation. Acta Biomater. 3, 873–881. https://doi.org/10.1016/j.actbio.2007.04.005

Gharravi, A.M., Orazizadeh, M., Hashemitabar, M., 2016. Fluid-induced low shear stress improves cartilage like tissue fabrication by encapsulating chondrocytes. Cell Tissue Bank. 17, 117–122. https://doi.org/10.1007/s10561-015-9529-2

Girão, A.F., Gonçalves, G., Bhangra, K.S., Phillips, J.B., Knowles, J., Irurueta, G., Singh, M.K., Bdkin, I., Completo, A., Marques, P.A.A.P., 2016. Electrostatic self-assembled graphene oxide-collagen scaffolds towards a three-dimensional microenvironment for biomimetic applications. R. Soc. Chem. Adv. 6, 49039–49051. https://doi.org/10.1039/C6RA10213A

Girão, A.F., Semitela, Â., Pereira, A.L., Completo, A., Marques, P.A.A.P., 2020. Microfabrication of a biomimetic arcade-like electrospun scaffold for cartilage tissue engineering applications. J. Mater. Sci. Mater. Med. 31, 69. https://doi.org/10.1007/s10856-020-06407-4

Girão, A.F., Semitela, Â., Ramalho, G., Completo, A., Marques, P.A.A.P., 2018. Mimicking nature: Fabrication of 3D anisotropic electrospun polycaprolactone scaffolds for cartilage tissue engineering applications. Compos. Part B Eng. 154, 99–107. https://doi.org/10.1016/j.compositesb.2018.08.001

He, X., Feng, B., Huang, C., Wang, H., Ge, Y., Hu, R., Yin, M., Xu, Z., Wang, W., Fu, W.,

Zheng, J., 2015. Electrospun gelatin/polycaprolactone nanofibrous membranes combined with a coculture of bone marrow stromal cells and chondrocytes for cartilage engineering. Int. J. Nanomedicine 10, 2089–2099. https://doi.org/10.2147/IJN.S79461

Hirsch, M.S., Cook, S.C., Killiany, R., Hartford Svoboda, K.K., 1996. Increased cell diameter precedes chondrocyte terminal differentiation, whereas cell-matrix attachment complex proteins appear constant. Anat. Rec. 244, 284–296. https://doi.org/10.1002/(SICI)1097-0185(199603)244:3<284::AID-AR2>3.0.CO;2-Z

J.-R. Delcroix, G., Molinari, M., Reiner, T., Thomas Temple, H., Valdes, M., B. Montero, R., M. Andreopoulos, F., C. Schiller, P., D'Ippolito, G., 2016. Multi-Layered Scaffold to Mimic Hyaline Articular Cartilage Architecture. Curr. Tissue Eng. 5, 21–28. https://doi.org/10.2174/2211542004666150713185804

Jeon, J.E., Schrobback, K., Hutmacher, D.W., Klein, T.J., 2012. Dynamic compression improves biosynthesis of human zonal chondrocytes from osteoarthritis patients. Osteoarthr. Cartil. 20, 906–915. https://doi.org/10.1016/j.joca.2012.04.019

Johnstone, B., Alini, M., Cucchiarini, M., Dodge, G.R., Eglin, D., Guilak, F., Madry, H., Mata, A., Mauck, R.L., Semino, C.E., Stoddart, M.J., 2013. Tissue engineering for articular cartilage repair – the state of the art. Eur. Cells Mater. 25, 248–267. https://doi.org/10.22203/eCM.v025a18

Jung, J.W., Lee, H., Hong, J.M., Park, J.H., Shim, J.H., Choi, T.H., Cho, D.W., 2015. A new method of fabricating a blend scaffold using an indirect three-dimensional printing technique. Biofabrication 7, 045003. https://doi.org/10.1088/1758-5090/7/4/045003

Ke, R., Yi, W., Tao, S., Wen, Y., Hongyu, Z., 2017. Electrospun PCL/gelatin composite nanofiber structures for effective guided bone regeneration membranes. Mater. Sci. Eng. C

78, 324–332. https://doi.org/10.1016/j.msec.2017.04.084

Kock, L., Van Donkelaar, C.C., Ito, K., 2012. Tissue engineering of functional articular cartilage: The current status. Cell Tissue Res. 347, 613–627. https://doi.org/10.1007/s00441-011-1243-1

Kostakova, E., Seps, M., Pokorny, P., Lukas, D., 2014. Study of polycaprolactone wet electrospinning process. Express Polym. Lett. 8, 554–564. https://doi.org/10.3144/expresspolymlett.2014.59

Levorson, E.J., Santoro, M., Kurtis Kasper, F., Mikos, A.G., 2014. Direct and indirect co-culture of chondrocytes and mesenchymal stem cells for the generation of polymer/extracellular matrix hybrid constructs. Acta Biomater. 10, 1824–1835. https://doi.org/10.1016/j.actbio.2013.12.026

Luo, L., O'Reilly, A.R., Thorpe, S.D., Buckley, C.T., Kelly, D.J., 2017. Engineering zonal cartilaginous tissue by modulating oxygen levels and mechanical cues through the depth of infrapatellar fat pad stem cell laden hydrogels. J. Tissue Eng. Regen. Med. 11, 2613–2628. https://doi.org/10.1002/term.2162

Makris, E.A., Gomoll, A.H., Malizos, K.N., Hu, J.C., Athanasiou, K.A., 2015. Repair and tissue engineering techniques for articular cartilage. Nat. Rev. Rheumatol. 11, 21–34. https://doi.org/10.1038/nrrheum.2014.157

Malekipour, F., Whitton, C., Oetomo, D., Lee, P.V.S., 2013. Shock absorbing ability of articular cartilage and subchondral bone under impact compression. J. Mech. Behav. Biomed. Mater. 26, 127–135. https://doi.org/10.1016/j.jmbbm.2013.05.005

McCoy, R.J., O'Brien, F.J., 2010. Influence of Shear Stress in Perfusion Bioreactor Cultures for the Development of Three-Dimensional Bone Tissue Constructs: A Review. Tissue Eng.

Part B Rev. 16, 587–601. https://doi.org/10.1089/ten.teb.2010.0370

McCullen, S.D., Autefage, H., Callanan, A., Gentleman, E., Stevens, M.M., 2012. Anisotropic fibrous scaffolds for articular cartilage regeneration. Tissue Eng. Part A 18, 2073–2083. https://doi.org/10.1089/ten.tea.2011.0606

Munir, N., McDonald, A., Callanan, A., 2020. Integrational Technologies for the Development of Three-Dimensional Scaffolds as Platforms in Cartilage Tissue Engineering. ACS Omega 5, 12623–12636. https://doi.org/10.1021/acsomega.9b04022

Pedraza, E., Brady, A.-C., Fraker, C.A., Stabler, C.L., 2013. Synthesis of macroporous poly(dimethylsiloxane) scaffolds for tissue engineering applications. J. Biomater. Sci. Polym. Ed. 24, 1041–1056. https://doi.org/10.1080/09205063.2012.735097

Powell, H.M., Boyce, S.T., 2009. Engineered human skin fabricated using electrospun collagen-PCL blends: morphogenesis and mechanical properties. Tissue Eng. Part A 15, 2177–2187. https://doi.org/10.1089/ten.tea.2008.0473

Rafiei, M., Jooybar, E., Abdekhodaie, M.J., Alvi, M., 2020. Construction of 3D fibrous PCL scaffolds by coaxial electrospinning for protein delivery. Mater. Sci. Eng. C 113. https://doi.org/10.1016/j.msec.2020.110913

Reboredo, J.W., Weigel, T., Steinert, A., Rackwitz, L., Rudert, M., Walles, H., 2016. Investigation of Migration and Differentiation of Human Mesenchymal Stem Cells on Five-Layered Collagenous Electrospun Scaffold Mimicking Native Cartilage Structure. Adv. Healthc. Mater. 5, 2191–2198. https://doi.org/10.1002/adhm.201600134

Remya, N.S., Nair, P.D., 2020. Matrix remodeling and mechanotransduction in in vitro chondrogenesis: Implications towards functional stem cell□based cartilage tissue engineering. Eng. Reports 2, 1–11. https://doi.org/10.1002/eng2.12145

Rnjak-Kovacina, J., Weiss, A.S., 2011. Increasing the pore size of electrospun scaffolds. Tissue Eng. Part B Rev. 17, 365–372. https://doi.org/10.1089/ten.teb.2011.0235

Sawatjui, N., Limpaiboon, T., Schrobback, K., Klein, T., 2018. Biomimetic scaffolds and dynamic compression enhance the properties of chondrocyte- and MSC-based tissue-engineered cartilage. J. Tissue Eng. Regen. Med. 12, 1220–1229. https://doi.org/10.1002/term.2653

Schuh, E., Kramer, J., Rohwedel, J., Notbohm, H., Müller, R., Gutsmann, T., Rotter, N., 2010. Effect of matrix elasticity on the maintenance of the chondrogenic phenotype. Tissue Eng. - Part A 16, 1281–1290. https://doi.org/10.1089/ten.tea.2009.0614

Semitela, Â., Girão, A.F., Fernandes, C., Ramalho, G., Bdikin, I., Completo, A., Marques, P.A.A.P., 2020. Electrospinning of bioactive polycaprolactone-gelatin nanofibres with increased pore size for cartilage tissue engineering applications. J. Biomater. Appl. 1–14. https://doi.org/10.1177/0885328220940194

Sheng, D., Li, J., Ai, C., Feng, S., Ying, T., Liu, X., Cai, J., Ding, X., Jin, W., Xu, H., Chen, J., Chen, S., 2019. Electrospun PCL/Gel-aligned scaffolds enhance the biomechanical strength in tendon repair. J. Mater. Chem. B. https://doi.org/10.1039/c9tb00837c

Shim, I.K., Suh, W.H., Lee, S.Y., Lee, S.H., Heo, S.J., Lee, M.C., Lee, S.J., 2009. Chitosan nano-/microfibrous double-layered membrane with rolled-up three-dimensional structures for chondrocyte cultivation. J. Biomed. Mater. Res. Part A 90A, 595–602. https://doi.org/10.1002/jbm.a.32109

Silva, M.L.A., Martins, A., Costa, P., Faria, S., Gomes, M., Reis, R.L., Neves, N.M., 2010. Cartilage tissue engineering using electrospun PCL nanofiber meshes and MSCs. Biomacromolecules 11, 3228–3236. https://doi.org/10.1021/bm100476r

Steele, J.A.M., McCullen, S.D., Callanan, A., Autefage, H., Accardi, M.A., Dini, D., Stevens, M.M., 2014. Combinatorial scaffold morphologies for zonal articular cartilage engineering. Acta Biomater. 10, 2065–2075. https://doi.org/10.1016/j.actbio.2013.12.030

Strobel, H.A., Calamari, E.L., Beliveau, A., Jain, A., Rolle, M.W., 2018. Fabrication and characterization of electrospun polycaprolactone and gelatin composite cuffs for tissue engineered blood vessels. J. Biomed. Mater. Res. - Part B Appl. Biomater. 106, 817–826. https://doi.org/10.1002/jbm.b.33871

Subia, B., Kundu, J., C., S., 2010. Biomaterial scaffold fabrication techniques for potential tissue engineering applications. Tissue Eng. 141–159. https://doi.org/10.5772/8581

Sun, B., Long, Y.Z., Zhang, H.D., Li, M.M., Duvail, J.L., Jiang, X.Y., Yin, H.L., 2014. Advances in three-dimensional nanofibrous macrostructures via electrospinning. Prog. Polym. Sci. 39, 862–890. https://doi.org/10.1016/j.progpolymsci.2013.06.002

Tan, G.Z., Zhou, Y., 2019. Electrospinning of biomimetic fibrous scaffolds for tissue engineering: a review. Int. J. Polym. Mater. Polym. Biomater. 0, 1–14. https://doi.org/10.1080/00914037.2019.1636248

Tarng, Y.W., Huang, B.F., Su, F.C., 2012. A novel recirculating flow-perfusion bioreactor for periosteal chondrogenesis. Int. Orthop. 36, 863–868. https://doi.org/10.1007/s00264-011-1291-x

Urbanek, O., Kołbuk, D., Wróbel, M., 2019. Articular cartilage: New directions and barriers of scaffolds development–review. Int. J. Polym. Mater. Polym. Biomater. 68, 396–410. https://doi.org/10.1080/00914037.2018.1452224

Wang, K., Zhu, M., Li, T., Zheng, W., Li, L., Xu, M., Zhao, Q., Kong, D., Wang, L., 2014. Improvement of cell infiltration in electrospun polycaprolactone scaffolds for the

construction of vascular grafts. J. Biomed. Nanotechnol. 10, 1–11. https://doi.org/10.1166/jbn.2014.1849

Wang, P.Y., Chow, H.H., Lai, J.Y., Liu, H.L., Tsai, W.B., 2009. Dynamic compression modulates chondrocyte proliferation and matrix biosynthesis in chitosan/gelatin scaffolds. J. Biomed. Mater. Res. - Part B Appl. Biomater. 91, 143–152. https://doi.org/10.1002/jbm.b.31384

Wang, W., Wan, Y., Fu, T., Zhou, T., Tang, X., Wu, H., Liu, C., Jagodzinski, M., 2019. Effect of cyclic compression on bone marrow mesenchymal stromal cells in tissue engineered cartilage scaffold. J. Biomed. Mater. Res. - Part A 107, 1294–1302. https://doi.org/10.1002/jbm.a.36642

Xue, J., Feng, B., Zheng, R., Lu, Y., Zhou, G., Liu, W., Cao, Y., Zhang, Y., Zhang, W.J., 2013. Engineering ear-shaped cartilage using electrospun fibrous membranes of gelatin/polycaprolactone. Biomaterials 34, 2624–2631. https://doi.org/10.1016/j.biomaterials.2012.12.011

Zhang, Q., Lu, H., Kawazoe, N., Chen, G., 2014. Pore size effect of collagen scaffolds on cartilage regeneration. Acta Biomater. 10, 2005–2013. https://doi.org/10.1016/j.actbio.2013.12.042

Zhang, Y., Liu, X., Zeng, L., Zhang, J., Zuo, J., Zou, J., Ding, J., Chen, X., 2019. Polymer Fiber Scaffolds for Bone and Cartilage Tissue Engineering. Adv. Funct. Mater. 29, 1903279. https://doi.org/10.1002/adfm.201903279

Zhang, Y., Ouyang, H., Chwee, T.L., Ramakrishna, S., Huang, Z.M., 2005. Electrospinning of gelatin fibers and gelatin/PCL composite fibrous scaffolds. J. Biomed. Mater. Res. - Part B Appl. Biomater. 72, 156–165. https://doi.org/10.1002/jbm.b.30128

Zhao, J., Griffin, M., Cai, J., Li, S., Bulter, P.E.M., Kalaskar, D.M., 2016. Bioreactors for tissue engineering: An update. Biochem. Eng. J. 109, 268–281. https://doi.org/10.1016/j.bej.2016.01.018

Zheng, R., Duan, H., Xue, J., Liu, Yu, Feng, B., Zhao, S., Zhu, Y., Liu, Yi, He, A., Zhang, W., Liu, W., Cao, Y., Zhou, G., 2014. The influence of Gelatin/PCL ratio and 3-D construct shape of electrospun membranes on cartilage regeneration. Biomaterials 35, 152–164. https://doi.org/10.1016/j.biomaterials.2013.09.082

Zhu, N., Che, X., 2013. Biofabrication of Tissue Scaffolds, in: Pignatello, R. (Ed.), Advances in Biomaterials Science and Biomedical Applications. InTech, Catania, Italy, p. 64. https://doi.org/10.5772/54125

Highlights

3D PCL+GEL porogenic fibrous scaffolds with anisotropic features were fabricated

Different depth-dependent fibrous alignments led to different mechanical responses

3D developed scaffolds generated an improved cell proliferation and infiltration

Mechanical stimulation enhanced cell proliferation and extracellular matrix build-up

Conflict of interest

☒ The authors declare that they have no known conflict interest or personal relationships that could have appeared to influence the work reported in this paper.